Journal of
Synchrotron Radiation

ISSN 1600-5775

Received 29 August 2014
Accepted 20 January 2015

On radiation damage in FIB-prepared softwood samples measured by scanning X-ray diffraction

Selina Storm,[a]* Malte Ogurreck,[b] Daniel Laipple,[b] Christina Krywka,[b] Manfred Burghammer,[c] Emanuela Di Cola[c] and Martin Müller[b]

[a]European Molecular Biology Laboratory (EMBL) Hamburg, c/o DESY, Notkestrasse 85, 22603 Hamburg, Germany, [b]Helmholtz-Zentrum Geesthacht, Zentrum für Material- und Küstenforschung GmbH, Max-Planck-Strasse 1, 21502 Geesthacht, Germany, and [c]European Synchrotron Radiation Facility, 6 rue Jules Horowitz, BP 220, 38043 Grenoble Cedex 9, France. *E-mail: selina.storm@embl-hamburg.de

The high flux density encountered in scanning X-ray nanodiffraction experiments can lead to severe radiation damage to biological samples. However, this technique is a suitable tool for investigating samples to high spatial resolution. The layered cell wall structure of softwood tracheids is an interesting system which has been extensively studied using this method. The tracheid cell has a complex geometry, which requires the sample to be prepared by cutting it perpendicularly to the cell wall axis. Focused ion beam (FIB) milling in combination with scanning electron microscopy allows precise alignment and cutting without splintering. Here, results of a scanning X-ray diffraction experiment performed on a biological sample prepared with a focused ion beam of gallium atoms are reported for the first time. It is shown that samples prepared and measured in this way suffer from the incorporation of gallium atoms up to a surprisingly large depth of 1 μm.

Keywords: FIB; radiation damage; scanning X-ray diffraction; nanodiffraction.

1. Introduction

Wood exhibits high mechanical strength combined with low density and is able to withstand constant and sometimes very changeable mechanical forces due to wind. Even though this material is extremely abundant in nature and has been studied intensively for decades (Page, 1976; Peltola *et al.*, 2000), several questions concerning the importance of the hierarchical wood structure for its unique mechanical properties still remain open. Many of them are related to the layered wood cell wall (Fengel & Wegener, 1983). Due to the semi-crystalline nature of the wood cell wall with cellulose nanocrystals, so-called microfibrils, embedded in a disordered matrix (Müller, 2009; Fernandes *et al.*, 2011), and the necessity to resolve individual cell wall layers with thicknesses down to about 100 nm (Donaldson & Xu, 2005), position-resolved X-ray scattering using synchrotron radiation has become a well established technique in this field over the last few years (Müller, 2009). Micro- and nanofocused synchrotron radiation X-rays, however, are characterized by a drastically increased flux density as compared with conventional X-ray tubes or even unfocused synchrotron radiation (Krywka & Müller, 2015). For biological materials, this means that radiation damage becomes an important issue. Apart from within the domain of protein crystallography there have been no extensive studies of radiation damage effects in high-flux sub-microbeam, mainly owing to the fact that true high-flux micro- and nanobeams have become available only very recently. Furthermore, the nature of the radiation damage occurring in biopolymers is still not completely clear. At the energies normally used in macromolecular crystallography, most of the X-ray energy deposited in the sample originates from photoelectric absorption (Ravelli & Garman, 2006). This leads to the emission of energetic electrons *via* the photoelectric, Auger and Compton effect.

While this direct interaction of the X-rays and electrons with the sample is known as primary radiation damage, the reactions of the resulting radiolytic products like free radicals and secondary lower-energy electrons cause the so-called secondary radiation damage (Teng & Moffat, 2000). Secondary radiation damage is time-dependent and can be reduced by cryo-cooling (Garman & Schneider, 1997). But even in cryo-cooled samples secondary lower-energy electrons can migrate to centres of high electronegativity and induce further damage (Yano *et al.*, 2005; Ravelli & Garman, 2006). The preparation procedure of thin wood cross sections (where softwood is used as a model system as it contains essentially only one cell type, the tracheid) turns out to be crucial for the exact determination of structural parameters on the hierarchical levels below the cell wall layers. In particular, the cell walls need to be precisely aligned parallel to the incident beam so that the three-dimensional orientation of the crystalline

cellulose microfibrils can be determined by X-ray diffraction (Lichtenegger *et al.*, 1999; Paris & Müller, 2003; Ogurreck & Müller, 2010). In previous experiments, (cryo) microtome sections were used (Lichtenegger *et al.*, 1999). However, the cell orientation is not well visible upon cutting. Subsequent alignment of the sections by means of optical microscopes and during the X-ray diffraction experiment is tedious and time-consuming. Thus, for the work presented here, focused gallium ion beam (FIB) milling was employed. Sample preparation by FIB milling allows an unprecedented accuracy regarding orientation by direct observation using FIB imaging or scanning electron microscopy (SEM). Splintering of the sample, which is a problem of cutting in a microtome, does not occur using a FIB. A drawback of the sample preparation with the FIB/SEM station used here is the damage to the surface of the sample by the gallium ions (Giannuzzi & Stevie, 1999). Both molecular dynamics simulations (Postawa *et al.*, 2004; Ziegler *et al.*, 2010) and experiments with metallic and biological FIB-milled samples (Maaß *et al.*, 2006; Marko *et al.*, 2007) refer to the incorporation of gallium as an interaction of primary ions and the sample as well as a redeposition up to a depth of the order of a few tens of nanometres. The extent of the incorporation and redepostion depend on the FIB-mill accelerating voltage, ion current and angle of incidence (Marko *et al.*, 2006; Stokes & Hayles, 2009).

In softwood nano-indentation experiments the formation of a 10 nm-thick skin has been reported, presumably caused by the interaction of gallium ions with the hemicellulose and lignin (Adusumalli *et al.*, 2010). In the present work the quality of the thin wood cross sections produced by FIB milling is evaluated. It will be determined whether the observed gallium incorporation into solid materials also holds true for softwood samples which contain large void areas (tracheid lumina). Additionally, the extent to which this sample preparation method is suitable to obtain spatially resolved information of the sample composition by means of subsequent X-ray diffraction will be evaluated. The different possible sources of radiation damage in wood, namely the scanning parameters with a focused X-ray beam and the additional influence of gallium in the scanning X-ray diffraction experiment, will also be addressed.

2. Materials and methods

2.1. Samples

Softwood exhibits a layered structure. In latewood samples of Norway spruce, the outer primary cell wall layer provides a thickness of 40–160 nm, followed by the three secondary cell wall layers S1 (190–710 nm), S2 (1.5–5.6 µm) and S3 (10–360 nm) (Fengel & Stoll, 1973). The latter is the last cell wall layer to be synthesized and borders the tracheid lumen. Depending on the cell wall layer, the ratio between the crystalline cellulose organized in microfibrils in the S1, S2 and S3 layers and the surrounding amorphous matrix varies. Furthermore, the microfibrils are rather disordered in the primary cell wall layer, while they are oriented parallel in the S2 layer (Plomion *et al.*, 2001).

2.2. Sample preparation

To investigate thin cell wall layers with X-ray diffraction in the way described above, the specimen must be prepared with very high accuracy regarding the perpendicularity of the tracheids longitudinal axis to the cutting direction. The required precise alignment and the perpendicular cut have been achieved with a FIB/SEM crossbeam workstation operated with gallium ions (AURIGA 40, Zeiss). Norway spruce samples provided by the Finnish Forest Research Institute Metla were initially cut with a scalpel to 3 mm × 5 mm sized pieces. These pieces were mounted with conductive silver glue onto a SEM sample holder to diminish the charging of the sample. Using the SEM, the orientation of the single wood cells becomes clearly visible and an area perpendicular to these cells can easily be defined. The specimens were cut at FIB currents of 10 nA and 20 nA and an acceleration voltage of 30 kV to achieve the desired lamella structure, requiring a milling time of about 24 h. A subsequent fine milling was performed at 2 nA to reduce beam damage, taking a milling time of at least 15 h. To cut the sample free, it was tilted to a 46° angle between sample and ion beam and a current of 10 nA was applied for at least 4 h. Then, the wood lamella was brazed to a manipulator (Omniprobe Autoprobe 200) using the gas injection system (Oxford Instruments) for depositing platinum, using a nominal FIB charge of 5 pAh µm^{-2}. Afterwards, the sample was removed and was fixed to the sample holder by using the gas injection system in the FIB-mill using the same settings. The last step increased the total milling time by about 4 h to at least 47 h: however, the total time for sample preparation totalled 50 h on account of the sample alignment and handling.

Sample A had a final size of 238 µm × 119 µm × 22 µm (Fig. 1*a*); sample B had a lateral size of 351 µm × 159 µm and was designed to have a thickness of 10 µm in the left and 15 µm in the right part of the sample (Fig. 1*b*). This was done

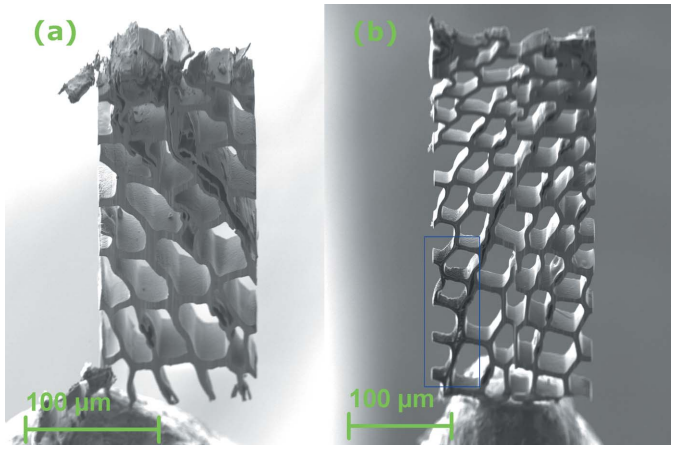

Figure 1
SEM pictures taken at an acceleration voltage of 2 keV of (*a*) sample A with a thickness of 22 µm and (*b*) sample B with a thickness of 10 µm for the left and 15 µm for the right part. The area surrounded by the blue box is thought to be the result of FIB damage and was therefore not investigated with scanning X-ray diffraction.

to obtain a more detailed picture of the local microfibril distribution and to determine a minimal required sample thickness for weakly scattering samples such as wood. The lower left part of sample B shows an irregular structure on the tracheids inner cell wall, which presumably is the result of FIB damage.

2.3. Scanning X-ray diffraction measurements

The measurement on sample A was performed at the nanofocus endstation of ID13 at the ESRF. The mounting of the sample was so accurate that almost no additional alignments were necessary. Fine-tuning of the sample orientation was performed with an *in situ* microscope installed at the experimental end-station. The X-ray beam with an energy of 14.9 keV was focused with nanofocusing refractive X-ray lenses to less than 100 nm × 100 nm. Significant scattering was recorded at an exposure of 0.5 s frame^{-1} with a FReLoN camera. The flux was of the order of 10^{11} photons s^{-1}. After some trials regarding the optimal step size, scanning was performed with a step size of 200 nm in the horizontal (H) and 400 nm in the vertical (V) direction. Under these conditions a mesh scan of 13.2 μm (H) and 20 μm (V) at the intersection point of three cells was performed.

The measurement on the thinner sample B was carried out at the nanofocus end-station of P03 at PETRA III (Krywka *et al.*, 2013). In this case the X-ray beam was focused to 250 nm (H) and 350 nm (V) using a KB mirror system at an energy of 14.7 keV. Using a PILATUS 1M detector the energy detection threshold was set to 12 keV. This feature is well suited for separating the gallium fluorescence from the diffraction signal. Sample B was mounted on a nanopositioner fixed on a hexapod, providing the possibility of aligning the sample with very high accuracy. Again, a microscope was used to align the sample. The first measurements took place in the 10 μm-thick area with a step size of 333 nm × 333 nm, with scanning in the vertical direction. The exposure was set to 10 s after taking into consideration the lower flux (10^9 photons s^{-1}) and the smaller projected thickness of the sample. Due to the fast propagation of X-ray radiation damage visible through the fading of the diffraction pattern in the sample, all line scans were separated by at least 1.5 μm. The 15 μm-thick area of the sample was scanned with a step size of 200 nm in the horizontal direction. For this measurement, an exposure time of 4 s was sufficient. To reduce the rate of radiation damage, cryo-cooling the sample was attempted. These trials failed due to the strong vibrations of the free-standing sample induced by the cryo-stream, making spatially resolved measurements impossible.

3. Results and discussion

In the first measurements, sample A was scanned with a step size of 200 nm (H) × 200 nm (V). In the diffraction patterns of the first row, both 200- and 110-reflections are visible, but the signal-to-noise ratio is worsening due to the propagation of secondary radiation damage (Fig. 2). Consequently the step size was increased to 200 nm (H) and 400 nm (V). At these scan settings the scattering signal of adjacent rows remained very similar.

In this way two complete cell walls of three adjacent cells could be scanned with the highest possible spatial resolution. The logarithmically scaled mesh shows a strong fluorescence signal at the edges of the sample (Fig. 3). By enlarging this

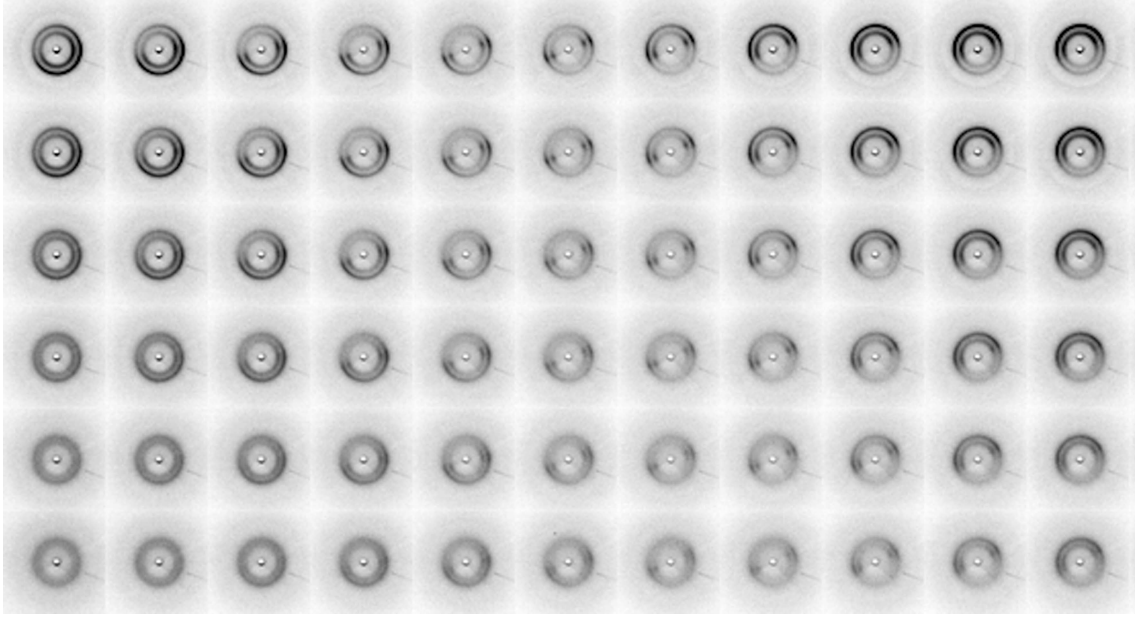

Figure 2
Diffraction images of sample A which were scanned with a step size of 200 nm × 200 nm, showing the 200-reflection in the outer and the 110-reflection in the inner ring. Data were recorded in lines, *i.e.* the scan direction is from left to right and from top to bottom. The fading of the diffraction signal due to radiation damage in the subsequent rows is clearly visible.

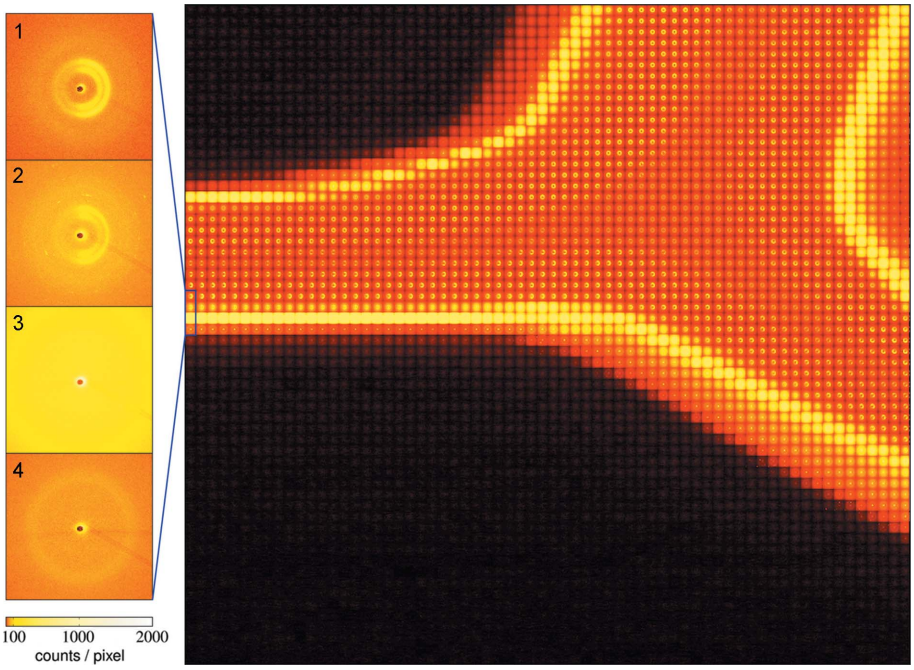

Figure 3
Composite image of the individual diffraction patterns of a cell wall intersection with a size of 13.2 µm (H) by 20 µm (V). The scanning step size was 200 nm (H) and 400 nm (V). The strong fluorescence signal and the complete disappearance of the cellulose reflections can be seen in the enlarged area, in images 1–4.

area, the weakening and finally the disappearance of the cellulose diffraction in the strong fluorescence in the third image from the top can be seen. Whatever scale was applied, the diffraction of the cellulose could not be made visible. Also, in the neighbouring images with lowest fluorescent signal, the reflections are broadened as the azimuthally integrated data show (Fig. 4), indicating strong local radiation damage. Owing to the disappearance of the diffraction patterns in the inner area of the cell walls, the thin S3 layer comprising one to two diffraction images cannot be separated from the broad S2 layer which is also partially affected. The signals from the S1 and the primary cell wall layers in the central part of the cell walls are less intense than from the S2 layer and are not visibly influenced by the sample preparation.

Softwood is mainly composed of carbon, oxygen and nitrogen, whose fluorescence emission lines do not exceed energies of 1 keV, and therefore are absorbed efficiently. The detected fluorescence must arise from the gallium incorporated during sample preparation. Because the gallium fluorescence is visible on all inner cell walls, it is likely that vapourized gallium ions redeposit on all surfaces, suggesting rather an environmental effect than the influence of the direct ion beam. In the latter case a strong direction-dependence would be expected. While the fluorescence seems to be more intense and closer to the surface in the left part of Fig. 3, it appears that the gallium ions seem to be incorporated deeper in the right-hand part of the sample which gives weaker fluorescence. This optical effect is created because the step size in the vertical direction is twice the size of that in the horizontal direction, and because the cell wall is probably not oriented fully parallel to the beam for the part of the sample shown in the lower right-hand part of Fig. 3. Nevertheless, judging from the intensity of the diffraction patterns, most gallium ions seem to be incorporated within a depth of about 1 µm.

Because it was thought possible to measure the diffraction patterns despite the strong fluorescence, a second experiment was performed at a similar incident X-ray energy. This time a PILATUS detector was available which allowed an energy threshold to be set above the fluorescent energy.

Measurements of the thinner sample B in the area with a thickness of 10 µm were also heavily affected by radiation damage. Despite the long exposure times of 4–10 s the diffraction signal was very weak, also due to the fact that the flux density was lower by a factor of 10^3 compared with the previous measurements at the ESRF. At room temperature, this gives rise to enhanced secondary radiation damage because the scan time has to be increased to acquire similar statistics, giving free radicals more time to propagate. This effect is visible in the weakening and the disappearance of the cellulose diffraction signal of adjacent rows. Since cryo-cooling turned out not to be an option for such mounted samples, and thus the spread of secondary radiation damage could not be reduced, line scans were

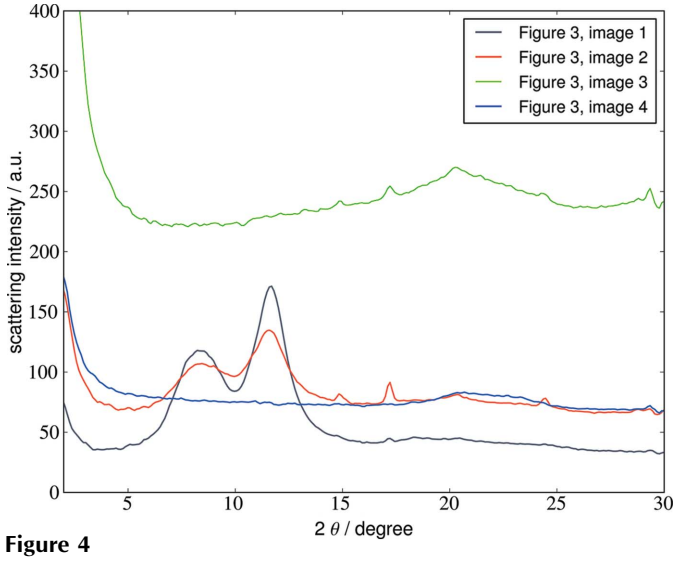

Figure 4
Azimuthally integrated intensity of the diffraction images shown in the enlarged area of Fig. 3 numbered from the top. In the third image, with the highest fluorescence, the diffraction of the cellulose has disappeared completely. The fourth image shows the same effect but was acquired at the very edge of the cell wall and the amount of sample material in the beam is very low, giving a much lower global signal strength.

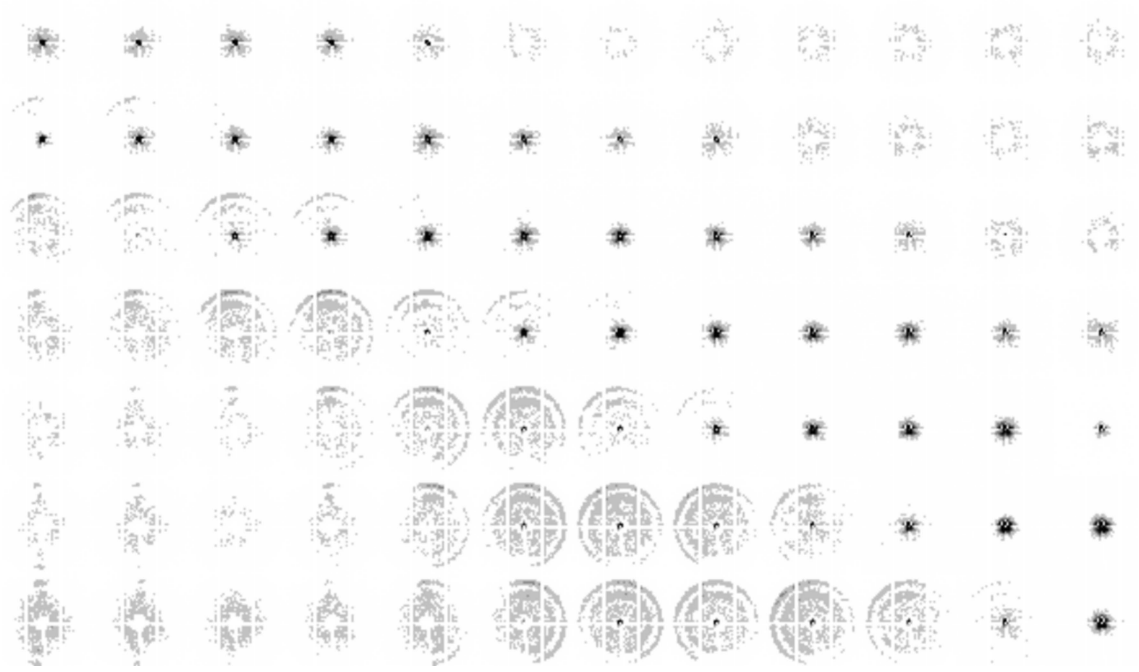

Figure 5
Diffraction patterns recorded with a step size of 0.2 μm × 1.5 μm. Using the PILATUS energy threshold the gallium fluorescence was not detected. In the areas where the gallium is incorporated, no cellulose scattering was signal detectable, but there was an enhanced small-angle scattering background.

performed over the 15 μm-thick area. When the gallium fluorescence was filtered out, no diffraction from the cellulose could be detected in the regions in which the gallium ions had passed or in which they seemed to be incorporated (Fig. 5). Additionally, enhanced small-angle X-ray scattering was detected in the regions in which the gallium ions were incorporated. As in sample A, the gallium ions were incorporated to a depth of up to 1 μm.

Two different effects may explain the disappearance of the cellulose diffraction. Firstly, it has been reported that gallium atom incorporation can lead to dislocations even in silicon (Maaß *et al.*, 2006). As the cellulose chains form crystals by weak hydrogen bonds and weak van der Waals interactions (Nishiyama *et al.*, 2002), the incorporation of gallium atoms may lead to disruption of these bonds. Since no reflections from wood are visible in the regions of strong gallium fluorescence, it can be deduced that gallium destroyed the crystallinity of the sample. The photoabsorption cross section of gallium exceeds that of carbon by a factor of 160 at an incident X-ray energy of 14.7 keV, leading to enhanced primary radiation damage in the region where gallium is incorporated. Also, the secondary radiation damage has to be considered.

For light elements such as carbon and oxygen, the Auger effect is dominant, resulting in a cascade of lower-energy secondary electrons which can migrate to areas with a high electron affinity such as metals and disulfide bonds (Yano *et al.*, 2005; Ravelli & Garman, 2006). In addition, the fluorescence yield increases for heavier elements, especially as the measurements here had to be performed above the absorption edge of gallium. The resulting fluorescence has an energy of 9.251 keV ($K_{\alpha1}$), 9.224 keV ($K_{\alpha2}$) and 10.264 keV ($K_{\beta1}$), giving rise to further damage to the sample. Probably a combination of the dislocations induced by the FIB and enhanced radiation damage due to the strong fluorescence at this energy takes place.

The number and the depth of the incorporated gallium ions is initially surprising, since, to the knowledge of the authors, all publications thus far report an incorporation depth of only some tens of nanometres. However, it should be noted that samples normally prepared with a FIB are a tenth or less of the size of the samples used in the current work, and also have a significant lower porosity (Reyntjens & Puers, 2001). For metals, an angle-dependent redeposition of gallium ions into the freshly milled sample has been reported, building an amorphous layer of up to 170 nm thick (Rubanov & Munroe, 2004). Moreover, it has been reported that wood becomes brittle when it is exposed to an electron beam (Hoffmeyer & Hanna, 1989). Even though there is no redeposition visible, the geometry of the FIB cut and the milling under two different angles, combined with long milling times and a brittle surface, could be reasons for the deep implementation and high concentration of gallium in the samples used here.

4. Conclusions

Investigation of a FIB-prepared biological sample by scanning X-ray nano-diffraction is reported here for the first time. Even though the samples were cut with an almost perfect orientation by using the FIB/SEM crossbeam station and well aligned at the beamline, the incorporation of the gallium ions into the sample poses problems for the investigation with scanning X-ray diffraction. At the incident X-ray energies used for

these measurements the gallium atoms give rise to a strong fluorescence signal. The strong fluorescence signal shows that the gallium ions are incorporated several times deeper into the sample than previously reported (Rubanov & Munroe, 2004; Maaß *et al.*, 2006; Marko *et al.*, 2007). To fully understand this effect, the behaviour of wood in FIB/SEM crossbeam stations needs to be further investigated. Furthermore, the influence of long milling times for biological samples of this size is another aspect which seems worthy of exploration. To lower the penetration depth of the gallium ions, the milling can be performed at lower voltage (Bassim *et al.*, 2012); however, this implicates even longer milling times. Additionally, the sample could be polished *via* argon beam milling (Erdman *et al.*, 2006).

The presence of gallium probably leads to dislocations of the weakly bound cellulose chains and to local radiation damage at the incident X-ray energies used. To rule out radiation damage being caused by gallium fluorescence, measurements could be carried out at lower energies. Generally it would be desirable to have other sample holders to fix the sample in such a way that cryo-cooling would be possible. By this means secondary radiation damage could be reduced, allowing for a smaller step size and better data at nanofocus beamlines with a lower flux.

Despite the damage to the S3 and parts of the S2 layer, the interior of the sample seems to be intact. Consequently this method can still be used to spatially investigate the primary, the S1 and parts of the S2 layers.

The authors thank Anja Glisovic for assistance during the ESRF beam time and Pekka Saranpää from the METLA for supplying the samples measured in these studies. Furthermore we gratefully acknowledge financial support from the German Research Foundation (DFG) *via* SFB 986 M^3, project Z2. We also sincerely thank the anonymous referees and Elspeth Garman for their comments, since these assisted in significantly improving our manuscript.

References

Adusumalli, R.-B., Raghavan, R., Ghisleni, R., Zimmermann, T. & Michler, J. (2010). *Appl. Phys. A*, **100**, 447–452.
Bassim, N., De Gregorio, B., Kilcoyne, A., Scott, K., Chou, T., Wirick, S., Cody, G. & Stroud, R. (2012). *J. Microsc.* **245**, 288–301.
Donaldson, L. & Xu, P. (2005). *Trees*, **19**, 644–653.
Erdman, N., Campbell, R. & Asahina, S. (2006). *Microsc. Today*, **14**, 22–25.
Fengel, D. & Stoll, M. (1973). *Holzforschung*, **27**, 1–7.
Fengel, D. & Wegener, G. (1983). *Wood: Chemistry, Ultrastructure, Reactions.* New York: Walter de Gruyter.
Fernandes, A. N., Thomas, L. H., Altaner, C. M., Callow, P., Forsyth, V. T., Apperley, D. C., Kennedy, C. J. & Jarvis, M. C. (2011). *Proc. Natl Acad. Sci. USA*, **108**, E1195–E1203.
Garman, E. F. & Schneider, T. R. (1997). *J. Appl. Cryst.* **30**, 211–237.
Giannuzzi, L. & Stevie, F. (1999). *Micron*, **30**, 197–204.
Hoffmeyer, P. & Hanna, R. (1989). *Wood Sci. Technol.* **23**, 211–214.
Krywka, C., Keckes, J., Storm, S., Buffet, A., Roth, S., Döhrmann, R. & Müller, M. (2013). *J. Phys. Conf. Ser.* **425**, 072021.
Krywka, C. & Müller, M. (2015). In *X-ray Diffraction: Modern Experimental Techniques*, edited by O. H. Seeck and B. Murphy. Singapore: Pan Stanford Publishing.
Lichtenegger, H., Müller, M., Paris, O., Riekel, C. & Fratzl, P. (1999). *J. Appl. Cryst.* **32**, 1127–1133.
Maaß, R., Grolimund, D., Van Petegem, S., Willimann, M., Jensen, M., Van Swygenhoven, H., Lehnert, T., Gijs, M., Volkert, C., Lilleodden, E. & Schwaiger, R. (2006). *Appl. Phys. Lett.* **89**, 151905.
Marko, M., Hsieh, C., Moberlychan, W., Mannella, C. & Frank, J. (2006). *J. Microsc.* **222**, 42–47.
Marko, M., Hsieh, C., Schalek, R., Frank, J. & Mannella, C. (2007). *Nat. Methods*, **4**, 215–217.
Müller, M. (2009). *Mater. Sci. Forum*, **599**, 107–125.
Nishiyama, Y., Langan, P. & Chanzy, H. (2002). *J. Am. Chem. Soc.* **124**, 9074–9082.
Ogurreck, M. & Müller, M. (2010). *J. Appl. Cryst.* **43**, 256–263.
Page, D. (1976). *Wood Fiber Sci.* **7**, 246–248.
Paris, O. & Müller, M. (2003). *Nucl. Instrum. Methods Phys. Res. B*, **200**, 390–396.
Peltola, H., Kellomäki, S., Hassinen, A. & Granander, M. (2000). *For. Ecol. Manag.* **135**, 143–153.
Plomion, C., Leprovost, G. & Stokes, A. (2001). *Plant Physiol.* **127**, 1513–1523.
Postawa, Z., Czerwinski, B., Szewczyk, M., Smiley, E. J., Winograd, N. & Garrison, B. J. (2004). *J. Phys. Chem. B*, **108**, 7831–7838.
Ravelli, R. B. G. & Garman, E. F. (2006). *Curr. Opin. Struct. Biol.* **16**, 624–629.
Reyntjens, S. & Puers, R. (2001). *J Micromech. Microeng.* **11**, 287.
Rubanov, S. & Munroe, P. (2004). *J. Microsc.* **214**, 213–221.
Stokes, D. J. & Hayles, M. F. (2009). *Proc. SPIE*, **7378**, 73780G.
Teng, T. & Moffat, K. (2000). *J. Synchrotron Rad.* **7**, 313–317.
Yano, J., Kern, J., Irrgang, K.-D., Latimer, M. J., Bergmann, U., Glatzel, P., Pushkar, Y., Biesiadka, J., Loll, B., Sauer, K., Messinger, J., Zouni, A. & Yachandra, V. K. (2005). *Proc. Natl Acad. Sci. USA*, **102**, 12047–12052.
Ziegler, J. F., Ziegler, M. & Biersack, J. (2010). *Nucl. Instrum. Methods Phys. Res. B*, **268**, 1818–1823.